Mid-infrared quantum cascade lasers

Maciej Bugajski, Dorota Pierścińska, Piotr Gutowski, Kamil Pierściński, Grzegorz Sobczak, Kamil Janus, Iwona Sankowska, Krzysztof Michalak, Krzysztof Chmielewski,
Joanna Branas, Aleksander Kuźmicz
Instytut Technologii Elektronowej, Al. Lotników 32/46, 02 668 Warszawa, Poland

ABSTRACT

We report recent results of works on quantum cascade lasers at the Institute of Electron Technology. During that time we have developed technology of lasers emitting at wavelengths 9.0–9.5 μm and 4.7 μm, based on InGaAs/AlGaAs/GaAs and InAlAs/InGaAs/InP heterostructures; both lattice matched and strain compensated. The structures were grown by molecular beam epitaxy MBE and by metalorganic vapor phase epitaxy MOVPE. The InGaAs/AlGaAs/GaAs lasers were grown by MBE. For InP based lasers three types of structures were investigated; the one grown exclusively by MBE without MOVPE overgrowth, the second fabricated by hybrid approach combining MBE grown AlInAs/InGaAs active region with MOVPE grown InP top waveguide layer and the third one with both the top and the bottom InP waveguide grown by MOVPE. Regardless of the waveguide construction, the active region was grown by MBE in every case. The lasers were fabricated in double trench geometry using standard processing technology. The buried heterostructure lasers were also investigated.

Keywords: Mid-infrared, quantum cascade laser

1. INTRODUCTION

We report recent results of works on quantum cascade lasers at the Institute of Electron Technology. During that time we have developed technology of lasers emitting at wavelengths 9.0–9.5 μm and 4.7 μm, based on InGaAs/AlGaAs/GaAs and InAlAs/InGaAs/InP heterostructures; both lattice matched and strain compensated. The structures were grown by molecular beam epitaxy MBE and by metalorganic vapor phase epitaxy MOVPE. The InGaAs/AlGaAs/GaAs lasers were grown by MBE. For InP based lasers three types of structures were investigated; the one grown exclusively by MBE without MOVPE overgrowth, the second fabricated by hybrid approach combining MBE grown AlInAs/InGaAs active region with MOVPE grown InP top waveguide layer and the third one with both the top and the bottom InP waveguide grown by MOVPE. Regardless of the waveguide construction, the active region was grown by MBE in every case. The lasers were fabricated in double trench geometry using standard processing technology. The buried heterostructure lasers were also investigated.

2. GaAs BASED QCLs

2.1. AlGaAs/GaAs (λ= 9.4 μm) lasers

The laser structure studied was the 36 period sequence of injector+3QW active region, made of $Al_{0.45}Ga_{0.55}As$/GaAs-coupled quantum wells. The active region was based upon the three quantum well design. The layer sequence of one period of the structure, in nanometers, starting from the injection barrier was: **4.6**, 1.9, **1.1**, 5.4, **1.1**, 4.8, **2.8**, 3.4, **1.7**, 3.0, **1.8**, 2.8, **2.0**, 3.0, **2.6**,3.0 nm. The AlGaAs layers are denoted in bold. The injector doping was on the level of $2x10^{17}cm^{-3}$. Only two barrier–QW pairs in the central part of each injector have been doped. The structure used double-plasmon Al-free waveguide for planar optical confinement. The core of the structure was embedded in the lightly doped waveguide composed of 3.5μm thick n-GaAs layers on each side ($n=4.0x10^{16}cm^{-3}$) terminated by 1μm thick highly Si doped ($n=1.0x10^{19}$ cm^{-3}) GaAs layers [8,9].

For epitaxial process control, the high resolution X-ray diffraction (HR XRD) and transmission electron microscopy (TEM) were used to characterize the morphological and structural properties of the layers. The XRD scan of the optimized QCL structure together with theoretical simulation is shown in Fig.1. The period thickness determined by

superlattice peaks spacing for this structure is 45.0 nm and the period thickness reproducibility from run to run is better than 1%. The calculated conduction band profile and moduli squared wavefunctions in injector/active/injector segment of the laser under the applied field of 48 kV/cm are shown in Fig.2. The position-resolved density of states (*color map*) is also shown. The population inversion between upper state 3 and lower state 2 is visible. This means that gain exist for applied bias. The calculations have been done by non-equilibrium Green's function (NEGF) method [12].

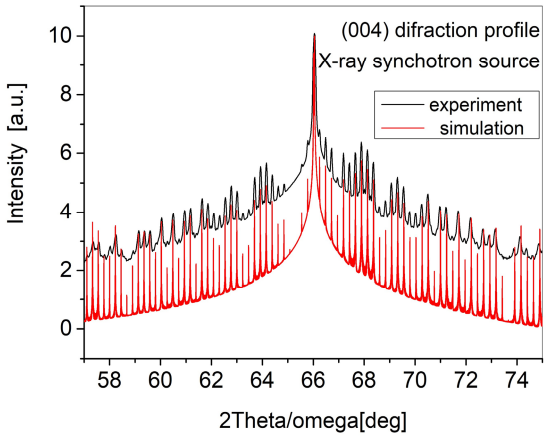

Fig.1 XRD scan for the GaAs/$Al_{0.45}Ga_{0.55}As$ QCL structure grown by MBE. The botom curve is theoretical one, calculated for planned structure. The large number of superlattice satelites is observed owing to the high quality of the structure.

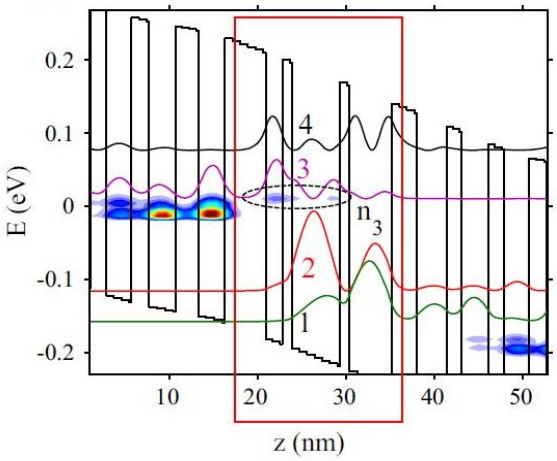

Fig.2 Conduction band profile and moduli squared wavefunctions in injector/active/injector segment of the laser under the applied field of 48 kV/cm. The level description: 3-upper laser level, 2-lower laser level, 1-depopulation level (after Ref.12)

The lasers were fabricated in double trench geometry using standard processing technology [10,11]. The exemplary light–current and current-voltage (L-I-V) characteristics of 9.4-μm $Al_{0.45}Ga_{0.55}As$/GaAs uncoated laser in pulse mode are shown in Fig.3. The characteristics were recorded in temperatue range from liquid nitrogen to room temperature. Maximum peak power delivered by the laser at liquid nitrogen temperature reaches 2.5 W. Lasers with broader mesa (~35 μm) were capable of delivering up to 6 W power. The rollover current, increases monotonically as a function of temperature. The parameters of $Al_{0.45}Ga_{0.55}As$/GaAs (λ= 9.4 μm) lasers are sumarized in Table 1.

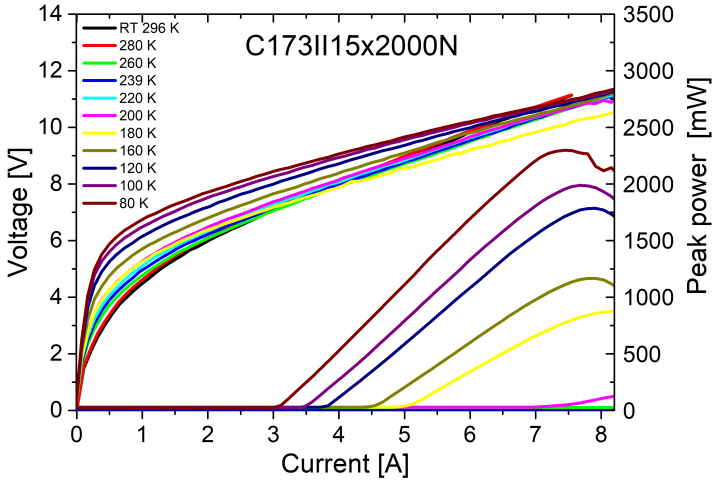

Fig.3 L-I-V characteristics of the $Al_{0.45}Ga_{0.55}As$/GaAs (λ= 9.4 μm) laser with uncoated facets, driven by 200 ns pulses with repetition rate of 5 kHz. The laser cavity length equals 2 mm and the mesa width equals 15 μm – after Ref.13.

Table 1. Parameters of $Al_{0.45}Ga_{0.55}As/GaAs$ (λ= 9.4 µm) lasers [13].

Parameter	Symbol	Value
Threshold current density	J_{th} (77K)	5 kA/cm^2 – 6 kA/cm^2
Threshold current density	J_{th} (300K)	10 kA/cm^2 - 15 kA/cm^2
Threshold voltage	V_{th} (77K)	~ 8.5 V
Pulse power	P (77K)	> 4 W (max 6 W)
Pulse power	P (300K)	25 mW – 35 mW
Wavelength	λ (300K)	~ 9.4 µm - 9.5 µm
Characteristic temperature	T_0	~ 90 K
Series resistance	R_s (77K-300K)	0.5 Ω – 0.7 Ω
Differential efficiency	η_d (77K)	0.8 W/A - 1.2 W/A
Wall plug efficiency	η_{wpe} (77K)	6 % - 8 %

2.2 InGaAs/AlGaAs/GaAs (λ= 9.2 µm) lasers.

A marked improvement of AlGaAs/GaAs lasers can be achieved by adding small ammounts of indium to GaAs quantum wells which results in an increase of conduction band discontinuity in InGaAs/AlGaAs heterostructure accompanied by decrease of interface roughness [5]. Because of the lattice mismatch between InGaAs and AlGaAs the In content can't be too high, but already ~3% In leads to substantial improvement of laser parameters. Above ~3% of In we observed lattice relaxation and decrease of material crystaline quality as documented by X-ray reciprocal space maps [14].

The comparison of L-I-V characteristics, for two QCL devices: standard GaAs/AlGaAs/GaAs and strained InGaAs/AlGaAs/GaAs is shown in Fig.4. The QCLs have the same cavity length and the mesa width of 2 mm and 25 µm, respectively. The devices were driven with 200 ns pulses with 5 kHz pulse repetition rate at the temperature of 77K and 250K. The latter was chosen such so the GaAs QCL would still emit some useful radiation.

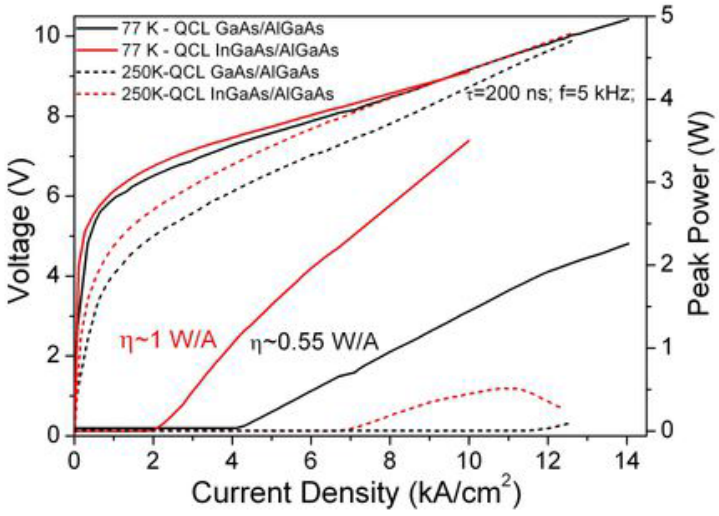

Fig.4 L-I-V characteristics of AlGaAs/GaAs laser (black lines) and $In_{0.03}Ga_{0.97}As/Al_{0.45}Ga_{0.55}As$ laser (red lines) at T=80K and T=250K. The lasers are driven in pulse mode with a repetition rate of 5 kHz and a pulse length of 200 ns.

From Fig.4 it follows immediately, that QCLs containing In outperform "standard" GaAs lasers. The advantage is gained in several aspects. Threshold current density has decreased by a factor of 2. It is also worth noting, that InGaAs/AlGaAs QCL operate at significantly lower voltages. Another improvement in case of InGaAs/AlGaAs QCLs is that they are characterised by higher slope efficiency of $\eta \approx 1$W/A per uncoated facet comparing to $\eta \approx 0.55$ W/A in case of GaAs/AlGaAs QCL. The emitted power in case of InGaAs/AlGaAs QCL is considerably higher, especially at elevated

temperatures. At 77 K for 5 A of supply current strained InGaAs/AlGaAs QCL emits 2.2 times more power than GaAs/AlGaAs QCL. At 250K for 6.5A supply current the difference is even more pronounced as emitted power is higher by a factor of ~5. This effect could be partially explained taking into account the electrical characteristics of those devices: lower current densities as well as lower voltage especially at higher values of supply current. Strained InGaAs/AlGaAs QCL emits radiation at much higher temperatures, reaching maximum working temperature of 323K (50^0C). Measured threshold current densities vs. temperature for both investigated QCL devices (black and red points) are presented in Fig. 5. Experimental data points were fitted using well-known expression for extraction of characteristic temperature J_{th}~exp(T/T_0) in the whole operating temperature range (77K-323K). Weaker temperature dependence of the threshold current density for InGaAs/AlGaAs is observed resulting in T_0=120K, as compared to more temperature sensitive AlGaAs/GaAs QCL, characterised by T_0=90K. The comparison of parameters of both types of lasers is presented in Table 2.

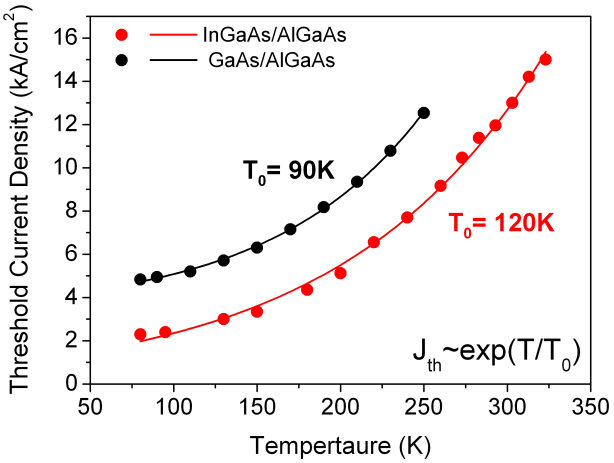

Fig.5 Temperature dependence of the threshold current density for AlGaAs/GaAs QCL (black line) and for $In_{0.03}Ga_{0.97}As$/ $Al_{0.47}Ga_{0.53}As$ QCL (red line).

Table 2. Parameters of $Al_{0.45}Ga_{0.55}As$/GaAs (λ= 9.4 μm) and $In_{0.03}Ga_{0.97}As/Al_{0.45}Ga_{0.55}As$/GaAs (λ= 9.2 μm) QCLs.

Parameter	AlGaAs/GaAs QCL	InGaAs/AlGaAs QCL
J_{th} (77 K) J_{th} (250 K)	4.2 (kA/cm^2) 13.3 (kA/cm^2)	2.2 (kA/cm^2) 7.3 (kA/cm^2)
T_0 (77 K-300 K)	90 (K)	120 (K)
WPE (77 K)	5.6 %	9.94 %
η (77 K)	0.6 W/A	1.3 W/A
Tmax	273 K (0 °C)	323 K (50 °C)
P (77 K) P (250 K)	2.2 W 90 mW	5.2 W 1.1 W

3. InP BASED QCLs

The bigest draback of mid-infrared GaAs based QCLs results from relatively low conduction band offset (~390 meV for $GaAs/Al_{0.45}Ga_{0.55}As$) and carrier escape from upper laser state to continuum at elevated temperatures. This causes a poor performance of GaAs/AlGaAs lasers at room temperature and excludes CW operation. Another consequence of small band offset is inability to move emission to shorter wavelength, in particular in the range of ~4 – 5 μm, interesting from point of view of applications in molecular spectroscopy. The rule of thumb is that the band offset should be roughly three times emission energy (ΔE≈3hν) to properly nest lower and upper laser levels in quantum wells. The problem can be solved by using InGaAs/InAlAs/InP structures which offer much higher band offset; ~520 meV in case of lattice

matched heterostructures and up to 800 meV in case of strain compensated heterostructures. The prize one pays, however, is greatly increased technological complexity. The material system, is based on two ternary compounds, InAlAs/InGaAs, which are not lattice matched to InP for all possible compositions except one. It requires high growth precision in terms of the composition and makes the analysis of the heterostructure parameters more difficult. Additionally, in strain compensated structures it is necessary to control compositions of four different ternary alloys in waveguide and active region during the growth.

The quantum cascade laser consists of two main elements; the cascade active region and the waveguide, which purpose is to confine electromagnetic field generated in the active region. Proper design of the waveguide is essential for the device operation and parameters such as threshold current and maximal working temperature.

In this work, three waveguide constructions were analyzed. The laser structures were grown either exclusively using MBE technology or by a combination of MBE and MOVPE technology. The schematic illustration of considered waveguide structures, marked from A to c, is shown in Fig.6. The growth method of specific layers is denoted on the left hand side of each diagram. Regardless of the waveguide construction, the active region was grown by MBE in every case, and utilized one of the discussed earlier active region designs.

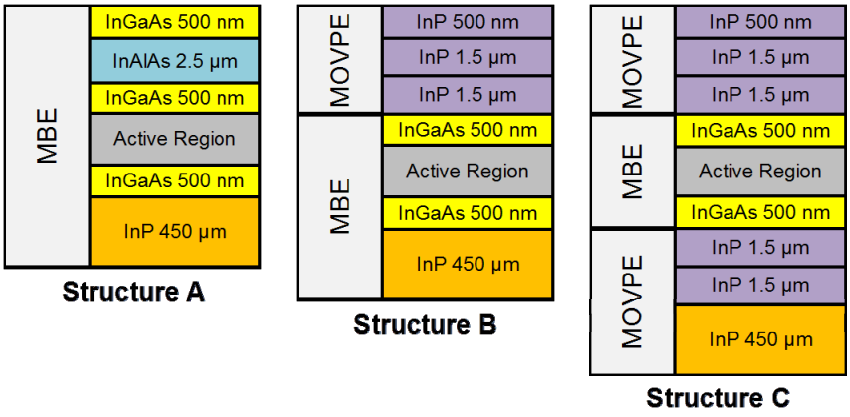

Fig.6 Schematic illustration of waveguide constructions grown in this work. The Structure A is single InAlAs waveguide, Structure B is single InP waveguide, Structure C is double InP waveguide

3.1 InGaAs/InAlAs/InP (~9.4 µm) lasers lattice matched to InP.

The lattice matched $Al_{0.477}In_{0.523}As/In_{0.533}Ga_{0.467}$ As/InP laser structures with 4-well 2-phonon resonance design were grown [16,17]. The layer sequence of one period of the structure, in nanometers, starting from the injection barrier is: **4.0**, 1.9, **0.7**, 5.8, **0.9**, 5.7, **0.9**, 5.0, **2.2**, 3.4, **1.4**, 3.3, **1.3**, 3.2, **1.5**, 3.1, **1.9,** 3.0, **2.3**, 2.9, **2.5, 2.9** nm. The AlInAs layers are denoted in bold. The total thickness of one period was 59.8 nm. The underlined layers were doped to $2x10^{17}cm^{-3}$. Single InAlAs waveguide was the simplest construction of QCL. It was grown entirely by MBE technology. The details of QCL construction are presented in Fig.7. Upper waveguide consists of 2.5 µm thick $In_{0.52}Al_{0.48}As$ layer and is terminated by highly doped 500 nm $In_{0.53}Ga_{0.47}As$ plasmon confinement layer. Bottom waveguide is formed by low doped substrate. Despite the drawbacks of this approach, such as high series resistance, high absorption losses and poor confinement factor, obtained lasers were characterized by a reasonably good operating parameters. The L-I-V characteristics for laser with 30 periods in the active region are presented in Fig.8.

In the Structure B, top InAlAs waveguide layer was replaced by InP grown by MOVPE. The active region has been grown by MBE, and then the wafer was transferred to MOVPE system for the growth of InP top waveguide and highly doped InP contact layer. The active region of laser consisted of 30 periods. Upper waveguide consist of two 1.5 µm thick InP sublayers with increasing doping and is terminated with highly doped 500 nm InP plasmon confinement layer. Bottom waveguide is formed by low doped substrate. The details of QCL construction and L-I-V characteristics are presented in Fig.9 and Fig.10, respectively.

500 nm	InGaAs	n=8×10^{18} cm^{-3}	Upper Waveguide
2.5 μm	InAlAs	n=1×10^{17} cm^{-3}	
500 nm	InGaAs	n=4×10^{16} cm^{-3}	
			Active Region
500 nm	InGaAs	n=4×10^{16} cm^{-3}	Lower Waveguide
450 μm	InP	n=2×10^{17} cm^{-3}	

Fig. 7 Single InAlAs waveguide (Structure A)

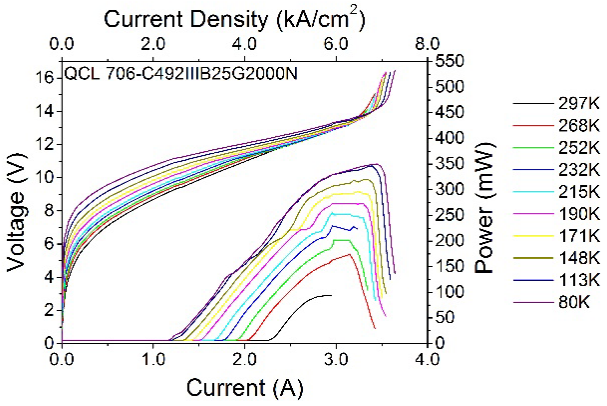

Fig.8 L-I-V characteristics of lattice matched $Al_{0.477}In_{0.523}As$/ $In_{0.533}Ga_{0.467}As$/InP QCL with 30 periods in the active region and single $In_{0.52}Al_{0.48}As$ waveguide (Structure A).

500 nm	InP	n=8×10^{18} cm^{-3}	Upper Waveguide
1.5 μm	InP	n=1×10^{17} cm^{-3}	
1.5 μm	InP	n=3×10^{16} cm^{-3}	
500 nm	InGaAs	n=4×10^{16} cm^{-3}	
			Active Region
500 nm	InGaAs	n=4×10^{16} cm^{-3}	Lower Waveguide
450 μm	InP	n=2×10^{17} cm^{-3}	

Rys.9 Dielectric slab waveguide formed by InP overgrowth process (Structure B).

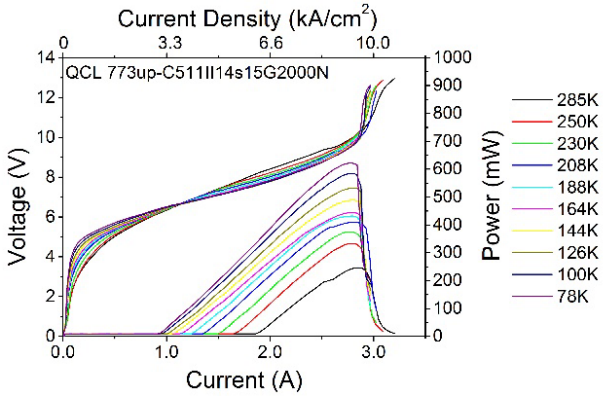

Fig. 10 L-I-V characteristics of lattice matched $Al_{0.477}In_{0.523}As$/ $In_{0.533}Ga_{0.467}As$/InP QCL with 30 periods in the active region and single single InP waveguide (Structure B).

Devices fabricated with InP overgrowth (Structure B) exhibited much better parameters than analogous devices based on single InAlAs waveguide configuration (Structure A). The reduction of threshold current and threshold voltage was observed with respect to MBE grown structures. Also, obtained slope efficiency and wall plug efficiency are much higher. Observed improvement results from the waveguide construction, which provides better optical mode confinement as well as improved thermal design. The latter stems from the fact, that InP thermal conductivity is higher than that of InAlAs roughly by a factor of 10. The lasers with 50 periods of active region were also grown. They have delivered much higher output powers as can be seen from Fig.11.

The comparison of threshold current densities for different the constructions of lattice matched QCLs is presented in Fig.12. A linear increase of the threshold current was observed, with the smallest being for single InP waveguide and the highest for single InAlAs waveguide.

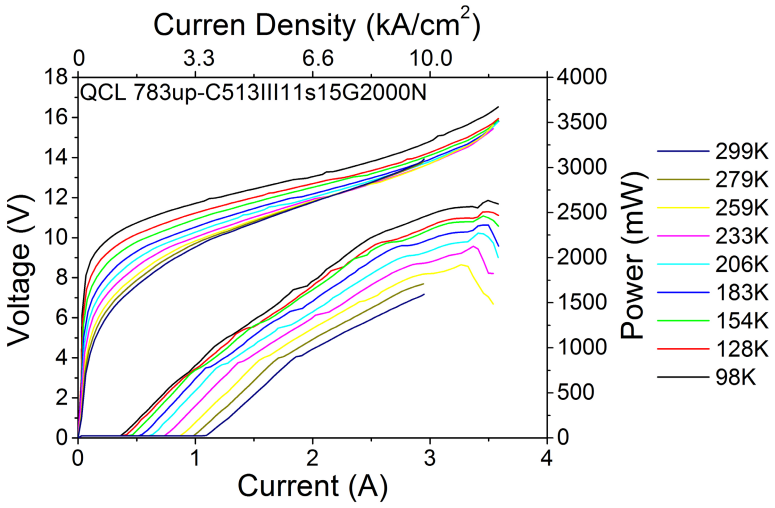

Fig.11 L-I-V characteristics for $Al_{0.477}In_{0.523}As/In_{0.533}Ga_{0.467}As$/InP QCL QCL with 50 periods in the active region and single InP waveguide (Structure B).

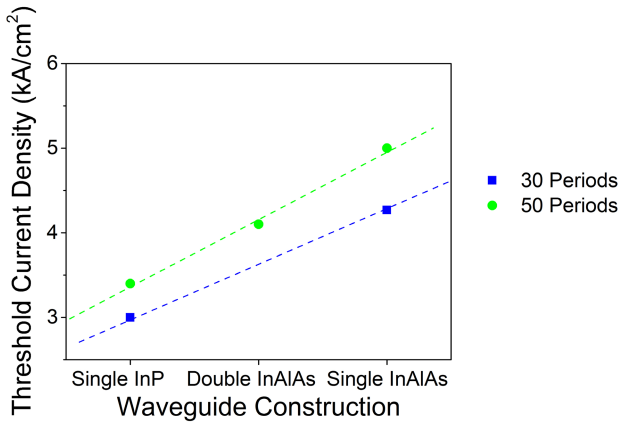

Fig.12 The dependence of threshold current density on waveguide construction for 30 and 50 period active region lasers.

Presented results show that waveguide construction based on low doped InP substrate with top InP waveguide grown by MOVPE was the best among the investigated ones. This is due to the best mode confinement factor and the highest thermal conductivity of the material, which guarantees good heat dissipation. Slightly worse results were obtained for the construction based on the low-doped InP substrate as lower waveguide and top InAlAs waveguide grown during the same process as the active region in the MBE reactor. Due to inferior thermal properties of this design, it did not reach the performance of InP top waveguide design. However for low duty cycles and short pulses the difference was not so pronounced. All lattice matched lasers operate well above room temperature (up to 100^0C) and deliver powers of the order of hundreds of mW which allows for their widespread application in environment protection, industry and medicine.

3.2 Strain compensated InGaAs/InAlAs/InP (~4.7 µm) lasers.

AlInAs/GaInAs/InP heterostructures can be also used for the construction of short wavelength laser emiting at around 5 µm. This is done by taking advantage of the modification of band structure of ternaries AlInAs and GaInAs caused by strain. $Ga_{0.467}In_{0.533}As/Al_{0.477}In_{0.523}As$/InP heterostructure is lattice matched to InP. When composition of ternareies deviates from the above the individual layers undergo biaxial deformation in the plane perpendicular to growth direction. The tensile strain in AlInAs barriers moves the conduction band edge to higher energies whereas a compressive strain in

InGaAs wells moves conduction band edge in opposite direction. As a result the conduction band offset in AlInAs/GaInAs heterostructure increases. An example of such structure is $Ga_{0.331}In_{0.669}As/Al_{0.638}In_{0.362}As$ for which conduction band offset is ~800 meV. In such a case, despite the ~1% lattice mismatch of individual layers the global strain is balanced and we deal with a pseudomorphic growth of the whole laser structure. On has to note, however that growth of such structures is the ultimate challenge for MBE.

The strain compensated $Al_{0.638}In_{0.362}As/In_{0.669}Ga_{0.331}$ As/InP laser structures consisted of the 35- segments. The active region of the lasers was of 4-well 2-phonon resonance design. The layer sequence of one period of the structure, in nanometers, starting from the injection barrier is: **3.8**, 1.2, **1.3**, 4.3, **1.3**, 3.8, **1.4**, 3.6, **2.2**, 2.8, **1.7**, 2.5, **1.8**, 2.2, **1.9**, 2.1, **2.1,** 2.0, **2.1**, 1.8, **2.7, 1.8** nm [7]. The AlInAs layers are denoted in bold. The total thickness of one period is 50.4 nm. The underlined layers are *n* doped to $2.5x10^{11}$ cm^{-2}. The strain-compensated QCLs were grown with three different waveguide designs: single InAlAs (Structure A), single InP (Structure B) and double InP (Structure C). It requires double sample transfer procedure between MBE and MOVPE systems. The heterostructures with strain-compensated active region are designed for shorter wavelengths (~4.7 μm). The L-I-V characteristics of strain compensated $Al_{0.638}In_{0.362}As/In_{0.669}Ga_{0.331}$ As/InP QCL with 35 periods in the active region and single $In_{0.52}Al_{0.48}As$ waveguide construction (Structure A) are shown in Fig.13.

The InGaAs/InAlAs/InP lasers emitting at 4.7 μm, with single InAlAs waveguide (Structure A), grown by MBE technology work in quasi-continuous mode (pulse length up to 10 μs) with powers above 0.5 W and exhibit room temperature threshold current densities 3.3 kA/cm^2. The lasers with single InP waveguide produced by MOVPE overgrowth (Structure B) show improved parameters but similarly to Structure A suffer from excess series resistance and absorption losses caused mainly by moderately doped substrate serving as bottom waveguide.

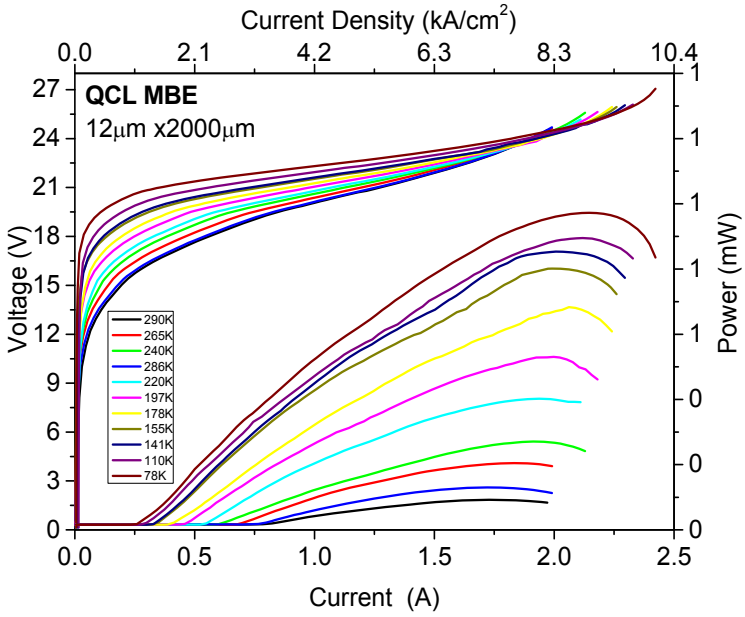

Fig.13 L-I-V characteristics of strain compensated $Al_{0.638}In_{0.362}As/In_{0.669}Ga_{0.331}$ As/InP QCL with 35 periods in the active region and single $In_{0.52}Al_{0.48}As$ waveguide construction (Structure A) – after Ref.7.

The L-I-V characteristics of strain compensated $Al_{0.638}In_{0.362}As/In_{0.669}Ga_{0.331}$ As/InP QCL with 35 periods in the active region and single InP waveguide construction (Structure B) are shown in Fig.14.

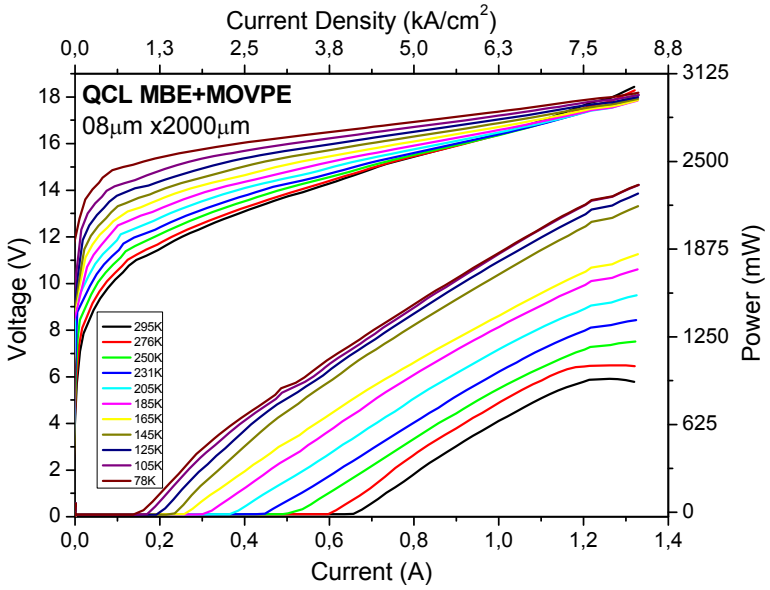

Fig.14 L-I-V characteristics of strain compensated $Al_{0.638}In_{0.362}As/In_{0.669}Ga_{0.331}$ As/InP QCL with 35 periods in the active region and single InP waveguide construction (Structure B).

The best parameters of the lasers have been achieved by using Structure C with symmetric InP waveguide. The fundamental TM mode profile in the structure is shown in Fig. 15. Waveguide losses have been determined experimentally. They were used as the input parameter of the model to calculate active region confinement factor and to calculate threshold gain. The TM_1 field is very well confined in the active region (Γ_{AR}=0.796) and its leakage to heavily doped contact layer is minimalized (Γ= 0.004). The total absorption losses are $\alpha_C = \alpha_W+\alpha_M = \alpha_{fc}+\alpha_S+\alpha_M$ = 5.948 cm^{-1} (L=4 mm). Taking estimated α_s = 1cm^{-1} (scattering losses at the interface roughness) and mirror losses α_M = (1/L)ln(1/R)=3.034 (L=4mm) one arrives with the threshold gain G_{th} =7.42 cm^{-1}, which is 3 times lower than the one for the laser with waveguide formed by the low doped substrate and the InAlAs layer [6].

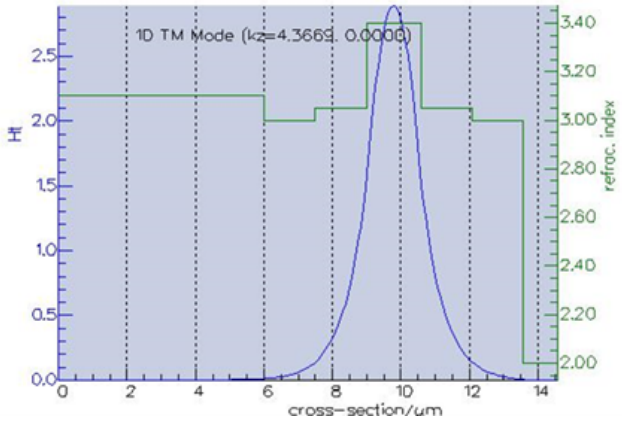

Fig.15 The fundamental TM mode profile in the $Al_{0.638}In_{0.362}As/In_{0.669}$ $Ga_{0.331}As$/InP laser structure (β=4.3571 μm^{-1}, n_{eff} + 3.2592, Γ) – after Ref.6

The L-I-V characteristics of strain compensated $Al_{0.638}In_{0.362}As/In_{0.669}Ga_{0.331}$ As/InP QCL with 35 periods in the active region and double InP waveguide construction (Structure C) are shown in Fig.16.

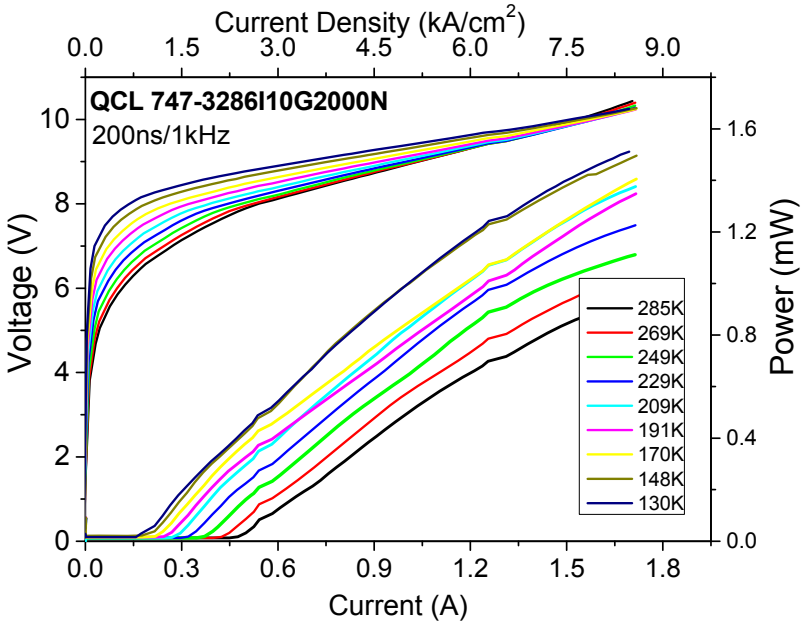

Fig.16 L-I-V characteristics of strain compensated $Al_{0.638}In_{0.362}As/In_{0.669}Ga_{0.331}As$/InP QCL with 35 periods in the active region and double InP waveguide construction (Structure C).

The parameters of lattice matched and strain compensated AlInAs/In_0GaAs/InP lasers are summarized in Table 3.

Table 3 The parameters of lattice matched and strain compensated AlInAs/In_0GaAs/InP lasers

		Lattice-matched QCL		Strain-compensated QCL	
Parameter	Symbol	*MBE*	*MBE+MOVPE*	*MBE*	*MBE+MOVPE*
Treshold current density	J_{th} (77K) [kA/cm²]	2,15	1,5	1,05	0,91
	J_{th} (295K) [kA/cm²]	4,6	3,3	3,3	2,3
Treshold voltage	V_{th} (77K) [V]	10,3	7,8	20,6	15,1
	V_{th} (295K) [V]	10,4	6,7	19,3	12,9
Characteristic T	T_0 [K]	135	170	128	154
	T_1 [K]	166	196	204	208
Max slope efficiency	η [W/A]	0,69	1,19	0,61	2,27

All so far discussed lasers were processed in double trench geometry. To improve thermal management of the lasers lattice matched InAlAs/InGaAs/InP structure with double InP waveguide (Structure C) was processed into buried Heterostructure lasers (BH QCL). After standard MOVPE overgrowth mesa structure was wet etched and then second MOVPE planarization overgrowth with semi-insulating InP:Fe has been performed. Resulting final structure is shown in Fig.17. Comparison of L-I-V characteristics of buried heterostructure and double trench lattice matched InAlAs/InGaAs/InP lasers (Structure C) is shown in Fig.18.

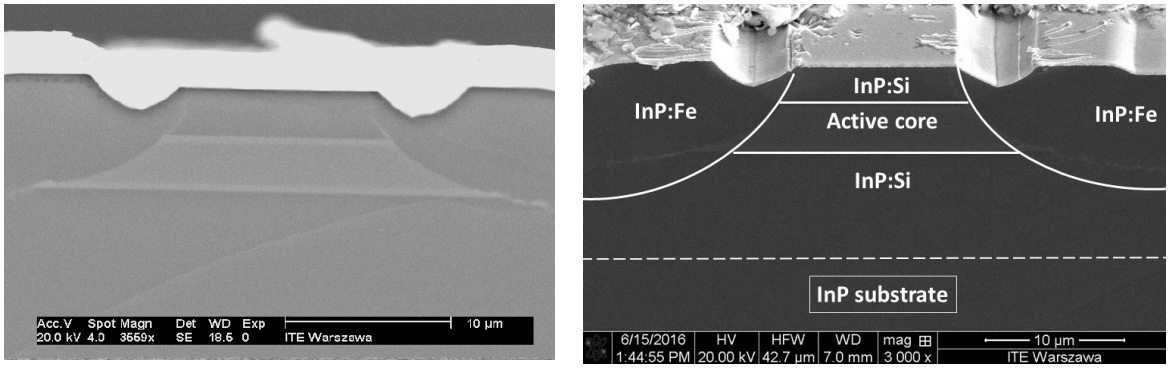

Fig.17 Scaning Electron Microscope (SEM) picture of BH QCL structure

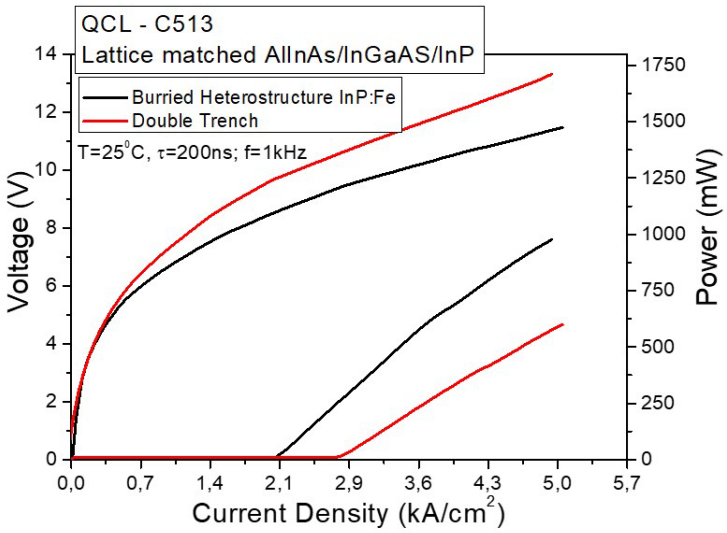

Fig.18 Comparison of L-I-V characteristics of buried heterostructure and double trench lattice matched InAlAs/InGaAs/InP lasers (Structure B).

The BH QCL exhibited low threshold current density J_{th}=2.1 kA/cm^2 and improved thermal behavior. When mounted epi-side down on copper submount they exhibited temperature rise in the active region in case of quasi-continuous operation at T=300 equal to 65 K. For epi-side up mounting the temperature rise was still only 85 K [18].

3. CONCLUSION

We report recent results of works on quantum cascade lasers at the Institute of Electron Technology. During that time we have developed technology of lasers emitting at wavelengths 9.0–9.5 µm and 4.7 µm, based on InGaAs/AlGaAs/GaAs and InAlAs/InGaAs/InP heterostructures; both lattice matched and strain compensated. The structures were grown by molecular beam epitaxy MBE and by metalorganic vapor phase epitaxy MOVPE. The InGaAs/AlGaAs/GaAs lasers were grown by MBE. For InP based lasers three types of structures were investigated; the one grown exclusively by MBE without MOVPE overgrowth, the remaining two fabricated by hybrid approach combining MBE grown InAlAs/InGaAs active region with MOVPE grown InP waveguide. All presented types of lasers exhibited parameters typical for their design and were successfully tested in prototype gas detection systems and free space communication systems.

Acknowledgements

The authors acknowledge contribution of M. Badura, B. Ściana and M. Tłaczała from Faculty of Microsystem Electronics and Photonics, Wrocław University of Science and Technology in MOVPE overgrowth technology.
The research has been founded by The National Centre for Research and Development NCBR under the project Techmatstrateg SENSE no. 1/347510/15/NCBR/2018 and by National Science Centre NCN under the project OPUS no. UMO-2015/17/B/ST7/04015.

Bibliography

1. J. Faist, F. Capasso, D. L. Sivco, C. Sirtori, A. Hutchinson, A. Y. Cho, Science 264, 553 (1994)
2. J. Faist, F. Capasso, C. Sirtori, D. L. Sivco, J. N. Baillargeon, A. Hutchinson, S. N. Chu, A. Y. Cho, Appl. Phys. Lett. 68, 3680 (1996)
3. C. Sirtori, P. Kruck, S. Barbieri, P. Collot, J. Nagle, M. Beck, J. Faist, U. Oesterle, Appl. Phys. Lett. 73, 3486 (1998)
4. C. Sirtori, P. Kruck, S. Barbieri, H. Page, J. Nagle, M. Beck, J. Faist, U. Oesterle, Appl. Phys. Lett. 75, 3911 (1999)
5. D. Pierścińska, P. Gutowski, G. Hałdaś, A. Kolek, I. Sankowska, J. Grzonka, J. Mizera, K. pierściński, M. Bugajski, "Above room temperaturę operation of InGaAs/AlGaAs/GaAs quantum cascade lasers", Semicond. Sci. Technol. **33**, 035006 (2017)
6. M. Bugajski, P. Gutowski, P. Karbownik, A. Kolek, G. Hałdaś, K. Pierściński, D. Pierścińska, J. Kubacka-Traczyk, I. Sankowska, A. Trajnerowicz, K. Kosiel, A. Szerling, J. Grzonka, K. Kurzydłowski, T. Slight, W. Meredith, "Mid-IR quantum cascade lasers: Device technology and non-equilibrium Green's function modeling of electro-optical characteristics" (invited paper), Physica Status Solidi (b) **251**, 1144–1157 (2014)
7. P. Gutowski, I. Sankowska, P. Karbownik, O. Serebrennikowa, M. Morawiec, E. Pruszyńska-Karbownik, K. Gołaszewska-Malec, D. Pierścińska, K. Pierściński, J. Muszalski, M. Bugajski, "MBE growth of strain compensated InGaAs/InAlAs/InP quantum cascade lasers", Journal of Crystal Growth **466**, 22-29 (2017)
8. K. Kosiel, M. Bugajski, A. Szerling, J. Kubacka-Traczyk, P. Karbownik, E. Pruszyńska-Karbownik, J. Muszalski, A. Łaszcz, P. Romanowski, M. Wasiak, W. Nakwaski, I. Makarowa, P. Perlin , "77 K operation of AlGaAs/GaAs Quantum Cascade Lasers", Photonics Letters of Poland **1**, 16 (2009)
9. K. Kosiel, A. Szerling, P. Karbownik, I. Sankowska, E. Pruszyńska-Karbownik, K. Pierściński, D. Pierścińska, P. Gutowski, M. Bugajski, "Room temperature AlGaAs/GaAs quantum cascade lasers", Photonics Letters of Poland **3**, 55-57 (2011)
10. A. Szerling, P. Karbownik, K. Kosiel, J. Kubacka-Traczyk, E. Pruszynska-Karbownik, M. Pluska, M. Bugajski, "Mid-Infrared GaAs/AlGaAs Quantum CascadeLasers Technology", Acta Phys. Polonica **116**, S45 (2009)
11. P. Karbownik, A. Baranska, A. Szerling, W. Macherzynski, E. Papis, K. Kosiel, M. Bugajski, M. Tlaczala, R. Jakieła, "Low resistance ohmic contacts to n-GaAs for application in GaAs/AlGaAs quantum cascade lasers", Optica Applicata, Vol. XXXIX, No. 4, 655 (2009)
12. G. Hałdaś, A. Kolek, D. Pierścińska, P. Gutowski, K. Pierściński, M. Bugajski, Opt. Quant. Electron. **49**, 22 (2017)
13. M. Bugajski, K. Kosiel, A. Szerling, P. Karbownik, K. Pierściński, D. Pierścińska, G. Hałdaś and A. Kolek, „High power AlGaAs/GaAs quantum cascade lasers" (invited paper), Proc. of SPIE Vol. 8432, 84320I (2012)
14. I. Sankowska, P. Gutowski, A. Jasik, K. Czuba, J. Dąbrowski, M. Bugajski, "On the onset of strain relaxation in the $Al_{0.45}Ga_{0.55}As/In_xGa_{1-x}As$ active region in quantum cascade laser structures", J. Appl. Crystallogr. **50**, 1376 (2017)
15. K. Pierściński, P. Gutowski, D. Pierścińska, P. Karbownik, M. Badura, O. Serebrennikova, I. Sankowska, M. Morawiec, D. Radziewicz, B. Ściana, E. Dumiszewska, M. Wesołowski, M. Tłaczała, W. Strupiński, M. Bugajski, "Strain compensated AlInAs/InGaAs/InP quantum cascade lasers", International Quantum Cascade Lasers School and Workshop, 4-9.09.2016, Cambridge, UK, paper no. 39
16. P. Gutowski, P. Karbownik, A. Trajnerowicz, K. Pierściński, D. Pierścińska, I. Sankowska, J. Kubacka-Traczyk, M. Sakowicz, M. Bugajski, "Room-temperature AlInAs/InGaAs/InP quantum cascade lasers", Photonics Letters of Poland **6**, nr. 3, (2014)
17. A. Kolek, G. Hałdaś, M. Bugajski, K. Pierściński, P. Gutowski, "Impact of Injector Doping on Threshold Current of Mid-Infrared Quantum Cascade Laser - Non-Equilibrium Green's Function Analysis", IEEE Journal of Selected Topics in Quantum Electronics **21**, 1200110 (2015)
18. D. Pierścinska, "Thermoreflectance spectroscopy – Analysis of thermal processes in semiconductor lasers" Journal of Physics D: Applied Physics **51** (2018) 013001